Study of Zn implanted silicon oxide films

© V.V. Privezentsev[1], A.P. Sergeev[1], A.A. Firsov[1], V.S. Kulikauskas[2],
E.E. Yakimov[3], E.P. Kirilenko[4], A.V. Goryachev[4]

[1] Federal Scientific Center Scientific Research Institute of System Analisys of the Russian Academy of Sciences,
Moscow, Russia
[2] Skobeltsyn Institute of Nuclear Physics, Lomonosov Moscow State University,
Moscow, Russia
[3] Institute of Technology of Microelectronics and High-Purity Materials, Russian Academy of Sciences,
Chernogolovka, Moscow region, Russia
[4] Institute of Nanotechnology of Microelectronics of the Russian Academy of Sciences,
Moscow, Russia

E-mail: v.privezentsev@mail.ru

This paper presents the results of studying the composition, structure, and properties of amorphous SiO_x film obtained by electron beam evaporation. This film was implanted by Zn ions with energy of 40 keV and a dose of $3 \cdot 10^{16}$ cm^2. Then, annealing was carried out in air at temperatures from 400 to 800°C with a step of 100°C for 40 min at each stage. It has been found that, after implantation, metal Zn nanoclusters with a size of about 10 nm are formed on the surface and in the near-surface layer of silicon oxide. During annealing, the implanted layer becomes enlightened, since metallic Zn gradually oxidizes to transparent phases of its oxide ZnO and silicide Zn_2SiO_4. After annealing at 700°C, ZnO nanoclusters and surface craters were revealed on the surface and in the subsurface layer of the SiO_2 film.

Keywords: silicon oxide film, electron beam evaporation, Zn implantation, thermal oxidation, nanoclusters, ZnO.

1. Introduction

In recent years, the properties of transition metals and their oxide nanoclusters (NCs) introduced into solid-state matrices have been comprehensively investigated because of their possible application in the development of modern optoelectronic and microelectronic devices [1–3]. Among them, a special role is played by the investigation of matrices with zinc oxide NCs, because this oxide is a directband material with a band gap of 3.37 eV, has a large binding energy between the electron and hole in the exciton (its value is 60 meV), is characterized by the sorption effect and can be classified as a piezoelectric and ferromagnetic material [4]. Therefore, zinc oxide nanoparticles can be widely used in light emitting devices of ultraviolet range [5], in solar cells [6], in gas sensors [7] and devices of spintronics [8], as well as in healthcare [9] and biology [10] sectors.

Currently, the investigation of zinc oxide gains a great importance due to the possibility to use it as a storage medium of the resistive random access memory (ReRAM). A ReRAM device [11], also known as memristor, is a simple structure: metal–dielectric–metal (MDM). Its operation principle is based on the reversible switching of dielectric material from the high resistance state to the low resistance state under the effect of current pulse. With a relatively simple geometry these devices have good performance

parameters, including nonvolatility, high switching rate (several ns), low operating current of about nA, scalability in the nm range and a potential memory of several bits with a large number of rewriting cycles ($> 10^{12}$). Currently, underway are studies of memristors based on a wide range of oxides of transition metals (TiO_2, HfO_2, ZrO_2, etc.) [12–14].

In a resistive memory element the low resistance state (LRS) of dielectric corresponds to either a state with high concentration of defects or a state with special mutual spatial arrangement of defects. Currently, the most discussed model of conducting channel formation in dielectric is based on the formation/dissociation of filament, a conductive channel with a diameter of $1-10$ nm [15,16]. In all appearances, defects are the factors that are responsible for such a transformation of the dielectric structure, because exactly on the defects the charge localization takes place, and concentration of defects should be sufficiently high: about 10^{19} cm^{-3} [17]. It is recognized that the most likely defects in oxides of transition metals and silicon oxides are oxygen vacancies [18]. It is supposed that the conductive filament is formed in a dielectric layer under a current pulse due to the exit and migration of oxygen atoms from lattice sites with the formation of oxygen vacancies [19]. With the resistive switching to the SET state, the current-conductive filaments are formed by continuous oxygen vacancies that bring the structure to the low-resistance state (LRS). In the

process of reverse switching (RESET), the oxygen vacancies recombine with oxygen ions and the device is switched to a state with high resistance of dielectric (HRS).

Recently, a great attention is paid to the process of creation and study of properties of memristors based on silicon oxide films [20] because silicon oxide is widely used in microelectronics and the technology of its formation is the most compatible with the technology of silicon integrated circuits. In particular, the effect of Si^+ ion implantation into the resistive-switching layer of SiO_x memristors followed by high-temperature heating has been studied. These processes have a significant effect on the structure of oxide film resulting in the formation of nanocrystalline inclusions, which promote the formation of conductive filaments [21]. In addition, it is found that parameters of a SiO_2-based memristor improve if cascades of silicon atom displacement are created and corresponding oxygen vacancies are formed in the near-surface layer of the SiO_2 film as a result of its irradiation by Xe^+ ions [22]. The enrichment of amorphous SiO_2 with oxygen vacancies has shown the possibility of silicon NC nucleation, which can play a significant role in the formation of conductive channels (filaments) and thus affect the memristor parameters.

In a number of studies attempts have been made to produce metal NCs by doping the silicon oxide with transition metal above the solubility limit. In particular, S.M. Sze and colleagues have shown [23–26] that thin films of amorphous SiO_x doped with Zn by the method of diffusion (so called SZO-films) in both single-layer and double-layer variants are promising materials for memristors thanks to the compatibility of their technology with the SMOS-technology. It has been found that these films have current-voltage curves ($C-V$ curves) corresponding to ReRAM devices, which are due to the presence of Zn or ZnO_x NCs, or, in general, Zn-containing cluster defects as the cause of such behavior of $C-V$ curves.

Of course, the investigation of SiO_2 films doped with zinc by other method for the use as an active layer of memristors is of importance as well. This study investigates zinc-implanted silicon oxide films. The method of implantation is the most clean and mobile technology of impurity injection into the target, which allows injecting large doses of impurity to different depths in the target at different energies of injection. The study has investigated structure, composition and properties of zinc-implanted films of SiO_2 produced by electron-beam vapor deposition for their possible use as an active layer of memristors. In particular, the process of formation of NCs of zinc and its oxides in the course of oxidation at high temperatures is investigated.

2. Samples and experimental procedure

The films were deposited using an electron beam setup with an oil-free pumping system and an electron gun that directly sputtering materials from a copper crucible cooled by running water. Chemically pre-cleaned quartz substrates with a thickness of 1 mm were heated to 250°C for degassing under vacuum of 10^{-6} mm Hg, and then the temperature was lowered to room temperature. Then the film of silicon oxide was deposited. The SiO_2 film was deposited at a pressure of $2 \cdot 10^{-5}$ mm Hg, with an accelerating voltage of 11 kV and a power of about 500 W. The rate of SiO_2 deposition was $1.5-2$ A/s and controlled by a quartz monitor. Thickness of the deposited SiO_2 film was 120 nm with an accuracy of 0.5 nm. Optical quartz of KU-1 grade was used as a charge for the process of film deposition. Then $^{64}Zn^+$ ions were implanted into the SiO_2/Au/quartz structures using an accelerator of heavy ions. Parameters of the implantation were as follows: energy was 40 keV and dose was $3 \cdot 10^{16}$ cm^{-2}, vacuum in the chamber was not worse than $1 \cdot 10^{-6}$ mm Hg. The ion current density was less than $0.35 \mu A/cm^2$, so the temperature of substrates in the process of implantation was not higher than 40°C. Them these structures were annealed in the air in the temperature range from 400 to 800°C with a step of 100°C, for 40 min at each step. On the zinc-implanted film of SiO_2, after appropriate annealing operations, circle aluminum electrodes with a diameter of 1.5 mm and a thickness of 100 nm were deposited through a mask.

The surface structure was investigated by scanning-electron microscope (SEM) using sensors of secondary electrons (SE) and back-scattered electrons (BSE) in combination with energy dispersive spectroscopy (EDS). The NCs of ZnO in the film were visualized by the method of cathodoluminscescence (CL), and the investigations were conducted using a SEM with a lattice of $300-850$ nm system and a resolution not worse than 2 nm.

The Auger spectra and profiles of elements were analyzed using an Auger spectrometer. The electron gun with a thermal field emission cathode (Schottky cathode) had an accelerating voltage of the primary electron beam of 5 kV; the primary electron current at spectra recording was 10 nA, and the current at SE and Auger-electron image recording was 2 nA. The tilt angle of the sample (the angle between the normal to the sample surface and the primary electron beam) was 60°. The energy of Ar ions for the profile analysis was 2 keV, the angle of etching was 49° in relation to the sample plane. The profiles were analyzed without rotation of the sample. Thickness of the layer was determined from the average sputtering rate after the crater depth measurement. The average deposition rate was determined with the profile analysis by a contact profilometer and was equal approximately to 10 nm/min.

3. Results and discussion

Fig. 1, *a* shows SEM-SE-image of the SiO_2 film surface after the implantation of Zn (the image has a mark on the scale of 2.5 μm). This SEM-SE-image has a low contrast. Light spots with a size of $50-200$ nm can be seen on the
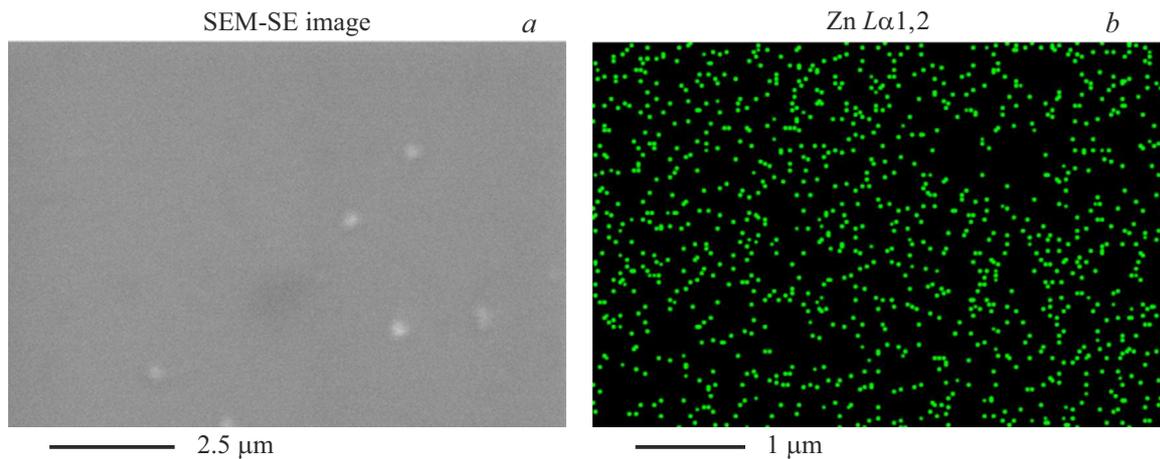
Figure 1. SEM image (*a*), EDS map for Zn Lα1, 2 (*b*) for the implanted sample.

SiO$_2$ film surface. These are small pimples on the surface of silicon oxide. Fig. 1, *b* shows EDS map of Zn for the sample of the zinc implantation. The EDS-spectrum of this sample has peaks that correspond to elements of the silicon oxide matrix, namely oxygen and silicon, as well as zinc (impurity) and carbon (contamination). Quantitative information for this sample is presented in the table.

Fig. 1, *b* shows EDS map of Zn distribution in the near-surface layer for the same frame as in Fig. 1, *a*. Also, EDS maps has been recorded for other elements (silicon, oxygen and carbon). It follows from the analysis of these maps that the distribution of implanted zinc, as well as elements of the matrix (silicon and oxygen) and carbon contamination is rather uniform, and we have failed to identify their precipitates. Thus, presumably a conclusion can be made that there are clusters on the sample surface that are composed of elements of the main SiO$_2$ matrix but perhaps they contain some implanted zinc. It may be concluded from the findings of the zinc-implanted bulk quartz investigation that if there are nanoclusters inside the SiO$_2$ film, their size is not more than 10 nm. In this case it is rather difficult to identify nanoclusters by the SEM method.

Fig. 2 shows SEM-SE-image of the implanted film surface after annealing at a temperature of 700°C for 40 min and corresponding EDS maps for elements. It can be seen in Fig. 2, *a* that light spots (pimples) and dark spots (craters) with a size of about 1 μm appear on the sample surface.

Content of elements in the SiO$_2$ film after implantation according to the EDS-spectrum

Element	Type of line	Content, at.%
Si	Kα1	20.48
O	Kα1	64.98
Zn	Lα1, 2	3.89
C	Kα1	10.6
Total		100.00

These craters are formed due to the backward diffusion of Zn into the ambient atmosphere in the process of high-temperature annealing. It follows from the comparison of Fig. 2, *a* and the map for Si, Fig. 2, *b*, that dark spots in Fig. 2, *a* have correspondent light spots in Fig. 2, *b*, and light spots in Fig. 2, *a* have correspondent dark spots in Fig. 2, *b*. To put it otherwise, craters correspond to an excess of Si and pimples correspond to lack of Si, i.e. they are not composed of Si. It follows from the comparison of Fig. 2, *a* and the map for O in Fig. 2, *b* that craters may be correspondent to both an excess of O (right hand part in Fig. 2, *c*) and a lack of O (left hand part in Fig. 2, *c*). However, the pimples in Fig. 2, *a* are correspondent to an excess of O in Fig. 2, *c*. The situation with zinc is completely different. It follows from the comparison of Fig. 2, *a* and the map fo Zn in Fig. 2, *b* that dark spots in Fig. 2, *a* have correspondent dark spots as well in Fig. 2, *c*, and light spots in Fig. 2, *a* have correspondent light spots in Fig. 2, *b*. To put it otherwise, craters correspond to a lack of Zn and pimples correspond to its excess. It follows from these considerations that craters in Fig. 2, *a* are arranged in the matrix of SiO$_2$ quartz and pimples are composed of zinc oxide, ZnO.

The study of sample surface after annealing at 700°C by the combination of SEM-SE and CL methods (Fig. 3) at low magnification shows that the annealed quartz surface has pimples with a size of several μm (Fig. 3, *a*). The recording of sample images with superposition of SEM-SE (Fig. 3, *a*) and CL (Fig. 3, *b*) signals in panchromatic mode [27] has identified features (light objects in Fig. 3, *b*) in the form of areas with a typical size of several μm. The arrangement of these light areas is in general correlated with pimples in the SEM-SE-image of the surface (Fig. 3, *a*), however, it should not be ruled out that some of them are located in the near-surface layer inside the sample as well. Taking into account that the SEM accelerating voltage was 15 keV, a conclusion can be made that these light agglomerates are located at a depth not more than 2 μm, however, in fact
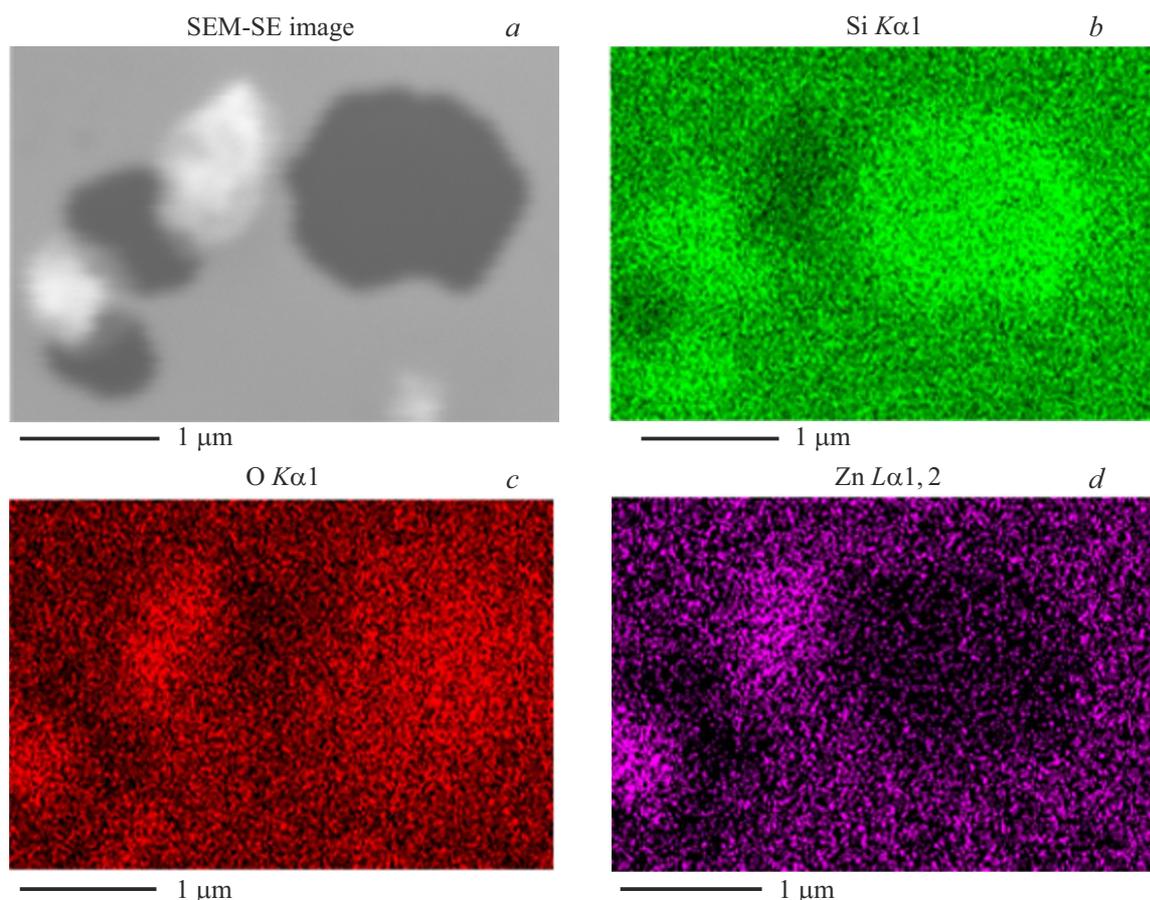
Figure 2. SEM-SE-image (*a*) and corresponding EDS maps for Si Kα1 (*b*), O Kα1 (*c*) and Zn Lα1, 2 (*d*) of the annealed sample.
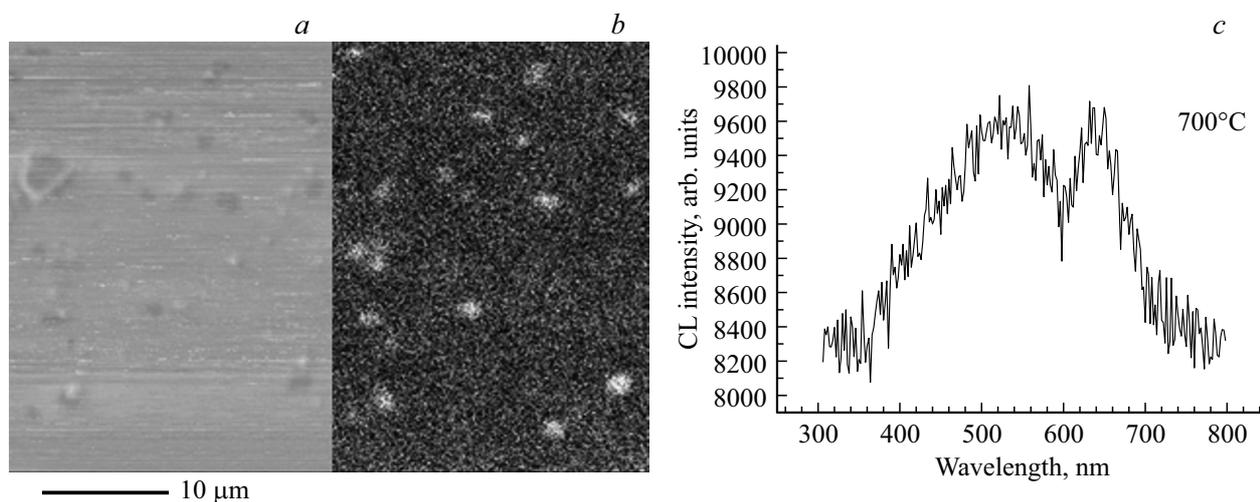
Figure 3. SEM-SE-image of the annealed sample (*a*), correspondent CL-image in the panchromatic mode (*b*) and CL spectrum of the sample annealed at 700°C (*c*).

they are located in the SiO$_2$ film at a depth of 20−60 nm where there is a sufficient amount of implanted zinc. Due to the features of the sample and the specific characteristics of the experimental setup it was impossible to measure the CL emission spectrum of an individual cluster. Fig. 3, *c* shows

emission spectrum of the sample, which image is shown in Fig. 3, *a*. It follows from the figure that two peaks in the CL spectrum at wavelengths of 540 and 640 nm are due to nonstoichiometric radiation defects in both the film of silicon oxide and the clusters of zinc oxide.
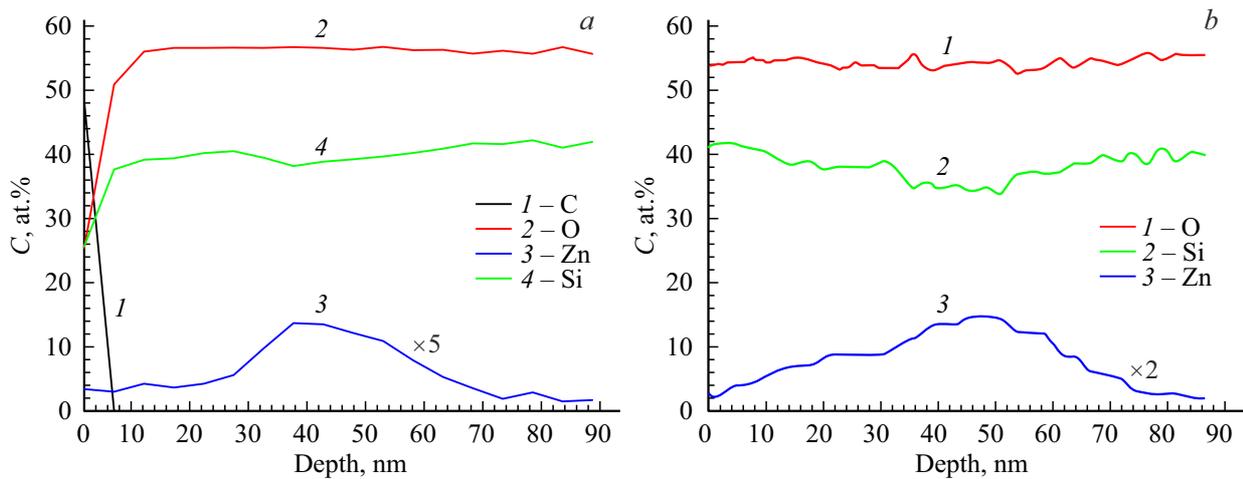
Figure 4. Concentration profiles of elements after Zn implantation (*a*) and after annealing at 700°C (*b*).
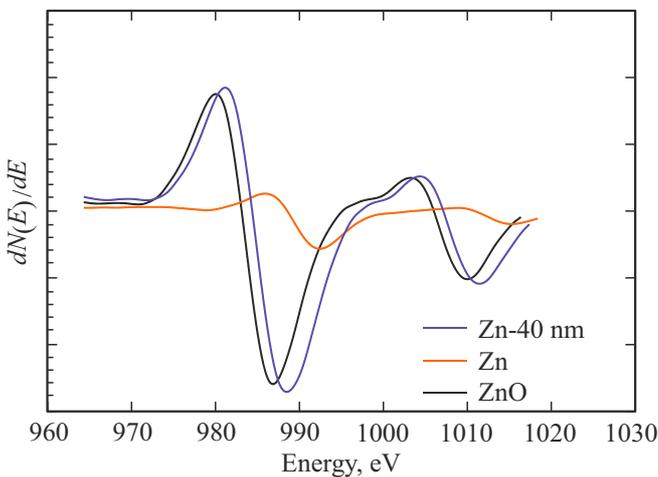
Figure 5. Differential Auger spectra of Zn at a depth of 40 nm for the implanted sample (Zn-40 nm — experimental, Zn and ZnO — references).

and „reference" spectra as a rule is used as „factors" in the AES interpreting. The analysis of Zn state in these samples used the reference spectra of Zn and ZnO from the database supplied together with the spectrometer. It is known [28] that the change in shape and energy of the Auger peak of a specific atom, depending on the chemical environment, takes place due to the change in the bond energy of electrons at the core level and due to the local density of states in the valence band. As a result of factor analysis [29], It has been found that after the implantation two zinc phases are formed in the zone of maximum zinc concentration (at a depth of 40 nm) : neutral (Zn°-phase, orange curve) and charged 2^+ (i. e. ZnO-phase, grey curve). Oxidation of zinc at the implantation occurs due to the break of Si-O bonds in the film of silicon oxide because of the implantation and the increase in temperature. Therefore, the released oxygen atoms interact with the implanted zinc

Fig. 4 shows concentration profiles of different elements obtained at an Auger spectrometer for the just implanted sample (*a*) and for this sample annealed at 700°C (*b*). It follows from Fig. 4, *a* that the top layer of the sample is covered with a film of hydrocarbons with a thickness of 5 nm. The distribution of implanted Zn is close to normal one with small tails, and the concentration peak is located at a depth of about 40 nm and does not exceed a few at.%. After annealing, the peak of Zn concentration profile is broadened in both sides but mainly toward the surface because it is an unlimited sink for the implanted zinc ions, however, peak of its distribution remains at approximately the same depth.

Fig. 5 shows the differential Auger electron spectrum (AES, blue) for the sample after Zn implantation. This spectrum can be decomposed into components by phases of Zn and ZnO. The comparison between experimental spectra

Figure 6. Differential Auger spectra of Zn at a depth of 40 nm for the sample annealed at 700°C (Zn-40 nm — experimental spectrum, Zn and ZnO — references).

and oxidize it to the ZnO phase. In other words, there is a mixture of two zinc phases, $Zn \times ZnO$, in this region of the sample.

Fig. 6 shows the differential AES spectrum (blue) for the sample after annealing at $700°C$. With the thermal annealing, molecules of oxygen diffuse into the film of silicon oxide, dissociate and almost completely oxidize the implanted zinc. At the same time, the Zn peak in the Auger spectrum at a depth of $40\,nm$ becomes less intensive as compared with the state after the implantation because the maximum of zinc concentration profile becomes somewhat lower. It was already mentioned above. Based upon the decomposition of the Auger spectrum into components by Zn and ZnO references, zinc in this region is completely in the ZnO phase, i. e. it has a charge of 2^+.

4. Conclusions

1. The maximum Zn concentration after the implantation is at a depth of about $40\,nm$ and does not exceed a few at.%.

2. After the implantation, Zn in the region of maximum concentration is the neutral state and in the 2^+ chemical state, i. e. a mixture of $Zn \times ZnO$ phases is formed.

3. After the annealing at $700°C$, in the region of concentration maximum at a depth of about $40\,nm$ Zn is in the 2^+ charge state, i. e. only the ZnO phase is formed.

4. After the annealing at $700°C$, the sample surface has clusters of ZnO and craters in the SiO_2 film with a size of about $1\,\mu m$.

Acknowledgments

Conflict of interest

The authors declare that they have no conflict of interest.

References

[1] M.I. Baraton. Synthesis. Functionalization, and Surface Treatment of Nanoparticles. Am. Sci., Los-Angeles (2002).

[2] T.C. Chang, K.C. Chang, T.M. Tsai, T.J. Chu, S.M. Sze. Mater. Today **19**, *5*, 254 (2016).

[3] C. Flytzanis, F. Haqche, M.C. Klein, D. Ricard, Ph. Roussignol. In: Prog. Opt. / Ed. E. Wolf. Amsterdam, North Holland **29**, 321 (1999).

[4] C.W. Litton, T.C. Collins, D.S. Reynolds. Zinc Oxide Materials for Electronic and Optoelectronic Device Application. Wiley, Chichester (2011).

[5] S. Chu, M. Olmedo, Zh. Yang, J. Kong, J. Liu. Appl. Phys. Lett. **93**, 181106 (2008).

[6] G.P. Smestad, M. Gratzel. J. Chem. Ed. **75**, 752 (1998).

[7] C. Li, Y. Yang, X.W. Sun, W. Lei, X. Zhang, B. Wang, J. Wang, B. Tay, J. Ye, G. Lo. Nanotechnology **18**, 135604 (2007).

[8] B.B. Straumal, A.A. Mazilkin, S.G. Protasova, E. Goering, G. Schütz, P.B. Straumal, B. Baretzky. Phys. Rev. B **79**, 205206 (2009).

[9] A. Sirelkhatim, S. Mahmud, A. Seeni, N.H.M. Kaus, L.C. Ann, S.K. ohd Bakhori, H. Hasan, D. Mohamad. Nano-Micro Lett. **7**, 219 (2015).

[10] S. Inbasekaran, R. Senthil, G. Ramamurthy, T.P. Sastry. Intern. J. Innov. Res. Sci. Eng. Technol. **3**, 8601 (2014).

[11] A. Mehonic, A.L. Shluger, D. Gao, I. Valov, E. Miranda, D. Ielmini, A. Bricalli, E. Ambrosi, C. Li, J.J. Yang, Q. Xia, A.J. Kenyon. Adv. Mater. **30**, *43*, 1801187 (2018).

[12] H. Yanqiu, L. Meidong, L. Zhen, Z. Yike, L. Shaobo. Mater. Sci. Eng. B **97**, *2*, 111 (2003).

[13] A. Garcia-Sotelo, M. Avila-Meza, M.A. Melendez-Lira, J.L. Fernandez-Muñoz, O. Zelaya-Angel. Mater. Res. **22**, *4*, e201901059 (2019).

[14] T. Torchynska, B. El Filali, G. Polupan, L. Shcherbyna. MRS Adv. **2**, 1 (2019).

[15] D.H. Kwon, KM. Kim, J.H. Jang, J.M. Jeon, M.H. Lee, G.H. Kim, X.S. Li, G.S. Park, B. Lee, S. Han, M. Kim, C.S. Hwang. Nature Nanotechnology **5**, 148 (2010).

[16] G. Bersuker, D.C. Gilmer, D. Veksler, P. Kirsch, L. Vandelli, A. Padovani, L. Larcher, K. McKenna, A. Shluger, V. Iglesias, M. Porti, M. Nafría. J. Appl. Phys. **110**, 124518 (2011).

[17] K. Xiong, J. Robertson, S.J. Clark. Phys. Status Solidi B **243**, 2071 (2006).

[18] M.V. Ganduglia-Pirovano, A. Hofmann. J. Sauer. Surf. Sci. Rep. **62**, 219 (2007).

[19] D.Z. Gao, A.-M. El-Sayed, A.L. Shluger. Nanotechnology **27**, *50*, 505207 (2016).

[20] N. Ilyas, C. Li, J. Wang, X. Jiang, H. Fu, F. Liu, D. Gu, Y. Jiang, W. Li. J. Phys. Chem. Lett. **13**, *3*, 884 (2022).

[21] E.V. Okulich, V.I. Okulich, D.I. Tetelbaum, A.N. Mikhaylov. Mater. Lett. **310**, 131494 (2022).

[22] E.V. Okulich, V.I. Okulich, D.I. Tetelbaum. Tech. Phys. Lett. **46**, *1*, 19 (2020).

[23] K.C. Chang, T.M. Tsai, T.C. Chang, H.H. Wu, J.H. Chen, Y.E. Syu, G.W. Chang, T.J. Chu, G.R. Liu, Y.T. Su, M.C. Chen, J.H. Pan, J.Y. Chen, C.W. Tung, H.C. Huang, Y.H. Tai, D.S. Gan, S.M. Sze. IEEE Eelecron. Dev. Lett. **34**, *3*, 399 (2013).

[24] K.C. Chang, T.M. Tsai, T.C. Chang, H.H. Wu, K.H. Chen, J.H. Chen, T.F. Young, T.J. Chu, J.Y. Chen, C.H. Pan, J.Y. Chen, C.W. Tung, H.C. Huang, Y.H. Tai, D.S. Gan, S.M. Sze. IEEE Electron. Dev. Lett. **34**, *4*, 511 (2013).

[25] R. Zhang, T.M. Tsai, T.C. Chang, K.C. Chang, K.H. Chen, J.C. Lou, T.F. Young, J.H. Chen, S.Y. Huang, M.C. Chen, C.C Shih, H.L. Chen, J.H. Pan, C.W. Tung, Y.E. Syu, S.M. Sze. J. Appl. Phys. **114**, 234501 (2013).

[26] J.S. Huang, W.C. Yen, S.M. Lin, C.Y. Lee, J. Wu, Z.M. Wang, T.S. Chin, Y.L. Chueh. J. Mater. Chem. C **2**, 4401 (2014).

[27] V.I. Petrov. Adv. Phys. Sci. **166**, *8*, 859 (1996).

[28] Surface Analysis by Auger and X-ray Photoelectron Spectroscopy / Eds D. Briggs, M.P. Sikh. Wiley, N.Y. (1983).

[29] Yu.B. Monakhova, S.P. Mushtakova. J. Anal. Chem. **67**, *12*, 1044 (2012).

Translated by Y.Alekseev